Protein Expression and Purification **17,** 324–338 (1999)
Article ID prep.1999.1111, available online at http://www.idealibrary.com on IDEAL®

Expression, Purification, and Structural Characterization of the Bacteriorhodopsin–Aspartyl Transcarbamylase Fusion Protein[1]

George J. Turner,*,[2] Larry J. W. Miercke,† Alok K. Mitra,‡ Robert M. Stroud,† Mary C. Betlach,†,[3] and Ann Winter-Vann*

**Department of Physiology & Biophysics, University of Miami School of Medicine, Miami, Florida 33101; †Department of Biochemistry & Biophysics, University of California at San Francisco, San Francisco, California 94143; and ‡Department of Cell Biology, The Scripps Research Institute, La Jolla, California 92037*

Received March 15, 1999, and in revised form May 14, 1999

We are testing a strategy for creating three-dimensional crystals of integral membrane proteins which involves the addition of a large soluble domain to the membrane protein to provide crystallization contacts. As a test of this strategy we designed a fusion between the membrane protein bacteriorhodopsin (BR) and the catalytic subunit of aspartyl transcarbamylase from *Escherichia coli.* The fusion protein (designated BRAT) was initially expressed in *E. coli* at 51 mg/liter of culture, to yield active aspartyl transcarbamylase and an unfolded bacterio-opsin (BO) component. In *Halobacterium salinarum,* BRAT was expressed at a yield of 7 mg/liter of culture and formed a high-density purple membrane. The visible absorption properties of BRAT were indistinguishable from those of BR, demonstrating that the fusion with aspartyl transcarbamylase had no effect on BR structure. Electron microscopy of BRAT membrane sheets showed that the fusion protein was trimeric and organized in a two-dimensional crystalline lattice similar to that in the BR purple membrane. Following solubilization and size-exclusion purification in sodium dodecyl sulfate, the BO portion of the fusion was quantitatively refolded in tetradecyl maltoside (TDM). Ultracentrifugation demonstrated that BR and BRAT–TDM mixed micelles had molecular masses of 138 and 162 kDa, respectively, with a stoichiometry of one protein per micelle. High TDM concentrations (>20 mM) were required to maintain BRAT solubility, hindering three-dimensional crystallization trials. We have demonstrated that BR can functionally accommodate massive C-terminal fusions and that these fusions may be expressed in quantities required for structural investigation in *H. salinarum.*

Key Words: **membrane protein; fusion protein; structure; bacteriorhodopsin; aspartyl transcarbamylase; expression system.**

Membrane proteins have been refractory to high-resolution structural analysis. The major obstacles to overcome in the pursuit of membrane protein structures include the inability to procure the quantities of membrane proteins required for crystallization and the limited diffraction properties of crystals when they have been obtained. Crystals useful for X-ray analysis have been obtained for only a few functionally distinct classes of membrane proteins: (i) the photoreaction centers and light harvesting complexes (1–4), (ii) the porins (5–7), (iii) an integral membrane enzyme, prostaglandin H2 synthase (8), (iv) cytochrome *c* oxidase (9), and (v) a potassium channel (10). As a result these are the only examples for which integral membrane components have been described at atomic level resolution.

[1] This work was supported by National Institutes of Health Grants GM14053 to G.J.T., GM31785 to M.C.B., and GM32079 to R.M.S. Support is also acknowledged in the form of an American Heart Association Grant-in-Aid (AHA664871) to G.J.T.

[2] To whom correspondence should be addressed at the Department of Physiology and Biophysics, P.O. Box 016430, The University of Miami School of Medicine, Miami, FL 33101. Fax: (305) 243-5931. E-mail: gturner@chroma.med.miami.edu.

[3] Current address: Kosan Biosciences, 3832 Bay Center Place, Hayward, CA 94545.

1046-5928/99 $30.00

Bacteriorhodopsin (BR)[4] remains a premiere model system for membrane protein structure–function analysis. BR is a complex of the apo-protein bacterio-opsin (BO) with retinal; its function is to generate an electrochemical potential via light-driven proton translocation across the cellular membrane in the halophilic Archaeon *Halobacterium salinarum* (11,12). The bacterio-opsin gene (*bop*) has been cloned (13) and has been transgenically expressed at high levels in both homologous (14–16) and heterologous (17,18) expression systems.

BR has been characterized extensively at the biophysical level and much has been revealed concerning the molecular transitions which mediate its photochemical function (see for reviews 19–21). *In vivo,* BR is organized as trimers in highly ordered two-dimensional lattices. Electron crystallographic analysis of these crystals revealed that the BR polypeptide chain is composed of seven transmembrane α-helices with retinal enclosed in the middle (22,23). A three-dimensional structure of BR had been obtained from electron crystallography, at a resolution of 3.5 Å in the plane of the membrane and 4.3 Å resolution normal to the bilayer (24). BR has attracted the attention of structural biologists as a candidate for high-resolution X-ray diffraction analysis for nearly 2 decades (25) and significant effort has been expended to obtain well ordered three-dimensional crystals in a crystallographically tractable space group (26). Recently, small three-dimensional isotropic crystals of BR were obtained by a lipid matrix nucleation procedure (27). The crystals diffracted to 2.0 Å in a synchrotron light source and a structure has been refined to 2.3 Å (28).

We are evaluating a different approach for membrane protein crystallization which employs molecular engineering to construct proteinaceous "crystallization tags." It is our hypothesis that crystal formation may be facilitated by protein-mediated crystal contacts and the addition of tags may promote ordered crystal growth. BR, for instance, contains very little extramembranous protein, and three-dimensional crystal growth must proceed in the absence of protein-mediated lattice contacts. As a first test of the utility of this strategy we have constructed a large polar domain for BR by gene fusion with a soluble protein, the catalytic subunit of the *Escherichia coli* aspartyl transcarbamylase (Fig. 1).

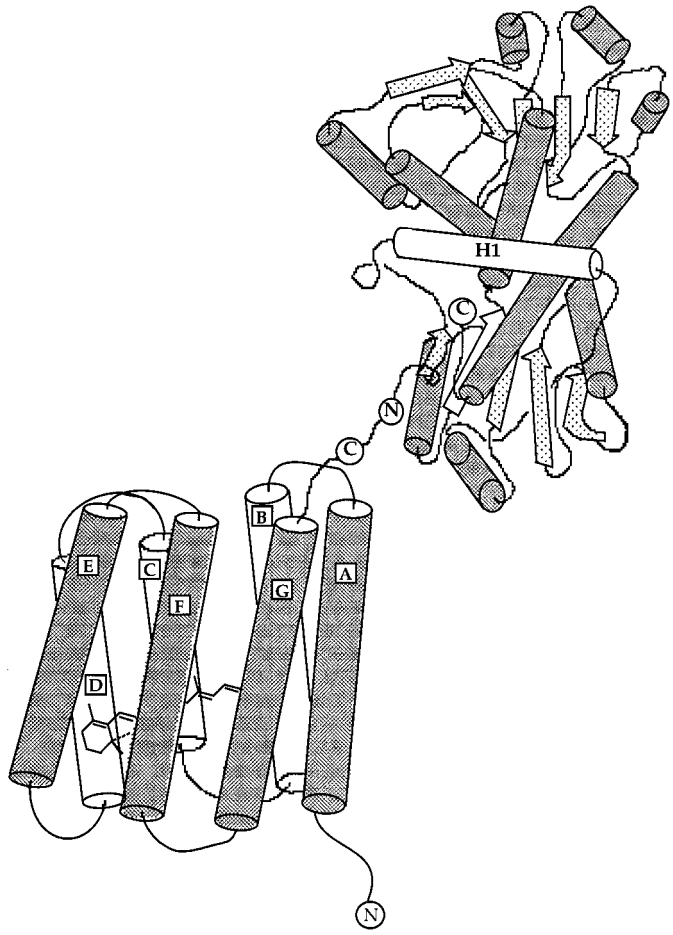

FIG. 1. Schematic monomeric representation of the bacteriorhodopsin–aspartyl transcarbamylase fusion protein, BRAT. Data from the BR model are from Henderson *et al.* (24). The seven transmembrane helices are labeled A through G. The ATCase model is from Ke *et al.* (39). The first helical segment is labeled H1. The N- and C-termini of both proteins are labeled N and C, respectively.

The *E. coli* aspartyl transcarbamylase holoenzyme is composed of 12 subunits, of two types, and catalyzes the formation of carbamyl aspartate and phosphate from aspartate and carbamyl phosphate (29). The larger subunits have a monomeric molecular mass of 33 kDa and spontaneously form trimers which possess the catalytic activity. The trimer can function independent of further macromolecular assembly (29,30).

In this report we describe the construction, high-level expression, and characterization of a fusion pro-

[4] Abbreviations used: ATCase, catalytic subunit of aspartyl transcarbamylase; BO, bacterio-opsin; BR, bacteriorhodopsin; BOAT, BO–ATCase fusion protein; BRAT, BR–ATCase fusion protein; e-BOAT, BO–ATCase fusion protein expressed in *E. coli;* h-BRAT, BR–ATCase fusion protein expressed in *H. salinarum;* PM, *H. salinarum* purple membranes harvested from sucrose gradients containing purified BR; BRATM, *H. salinarum* membranes harvested from sucrose gradients containing purified BRAT; IPTG, isopropyl-β-D-thiogalactopyranoside; SM-Glucose, glucose-supplemented M9 salts; YT, yeast extract tryptone; cfu, colony-forming units; FXa, blood clotting proteinase Factor Xa; NG, nonyl glucoside; Chapso, 3-[cholamidopropyldimethylammonio]-2-hydroxyl-1-propanesulfonic acid; Chaps, 3-[cholamidopropyldimethylammonio]-2-hydroxyl-1-propane sulfonate; βME, β-mercaptoethanol; HPSEC, high-performance size-exclusion chromatography; DMPC, dimyristoylphosphotidylcholine; TDM, tetradecyl maltoside; DA, dark-adapted.

tein composed of BR and the catalytic subunit of aspartyl transcarbamylase (subsequently referred to as ATCase). The fusion protein (referred to hereafter as BRAT) was expressed, at high level, in both *E. coli* and *H. salinarum*. Electron diffraction demonstrated that near-native quaternary structures of BR and ATCase are maintained in the fusion. These efforts show the feasibility of expressing multiple-milligram quantities of BR fusion proteins, containing large C-terminal extensions. This work also introduces a strategy for supplying crystallization contacts to membrane proteins, which may contribute to the goal of obtaining high-resolution structures of integral membrane proteins.

MATERIALS AND METHODS

Bacterial Strains

E. coli K12 strains used were the HB101 derivative D12·10 (*leuB6, proA2, recA13, lacY1, ara14, galK2, xyl5, mtl1, rpsL20, supE44, hsdS20, lacI^q*, l$^-$, F$^-$; 31), NCM533 (*lacZ*::Tn*5, lacI^{q1}*, l$^+$; provided by J. Keener and S. Kustu, University of California, Berkeley), DH5α (F$^-$, *recA1, endA1, gyrA96, thi-1, hsdR17* (r^-_k, m^+_k), *supE44*, l$^-$), and U39a (F$^-$, *ara*, Δ*lac-pro*), *strA, thi*, Δ*pyrB, rpsL* provided by J. Wild). Haloarchaeal strains were ET1001 (*Vac*$^-$, *BR*$^{+++}$, *Rub*$^-$; 32) and L33 (*Vac*$^-$, *BR*$^-$, *Rub*$^-$; 33).

Media and Growth Conditions

All salts and chemicals were reagent grade. Bacteriological peptone was from Oxoid, Unipath Ltd. (Hampshire, England), yeast extract tryptone, peptone, and Bacto-Agar were from Difco Laboratories (Detroit, MI).

Complex haloarchaeal medium was basal salts plus peptone or yeast extract tryptone (34). *H. salinarum* cells were transformed as described previously (15,16). Selective media included 10–25 μM mevinolin (gift from A. W. Alberts; Merck, Sharp and Dohme, Rathaway, NJ).

Complex *E. coli* medium was YT (35) and minimal medium was M9 salts (36) containing 0.4% (v/v) glycerol and supplemented with 1.0 mM $FeCl_3$ and 0.2 mg/ml thiamin. *In vivo* complementation analysis was performed in M9 salts containing 0.4% (v/v) glucose (SM-Glucose) combinatorially supplemented with IPTG, proline, and uracil (36).

Growth was monitored spectrophotometrically, at λ_{600} for *E. coli* cultures and at λ_{660} for *H. salinarum* cultures, using a Beckman DU-50 spectrophotometer. The absorbance readings were correlated with colony-forming units (cfu) per milliliter as determined by the plate spreading assay (16).

Vectors

Reagents. T4 DNA ligase and various restriction endonucleases were purchased from New England Biolabs (Beverly, MA) or from Boehringer Mannheim (Indianapolis, IN). Klenow fragment of DNA polymerase I was from Bethesda Research Labs (Gaithersburg, MD). *Taq* Polymerase was obtained from Perkin–Elmer (Norwalk, CT) Deoxynucleoside triphosphates were from Pharmacia (Piscataway, NJ). Wizard DNA miniprep kit was from Promega Corporation (Madison, WI). Preparative DNA isolation was by the protocols of Qiagen (Chatsworth, CA). Custom oligo-deoxynucleotides were purchased from Gibco. Oligo-directed mutagenesis was performed with the Transformer Site-Directed Mutagenesis kit, Clontech Laboratories, Inc. (Palo Alto, CA). DNA sequencing was accomplished by Sequenase protocols, United States Biochemical (Cleveland, OH). RNA was isolated by RNA-Stat 60 extraction (Tel-Test, Inc., Friendswood, TX) or the RNeasy Total RNA method (Qiagen). Digoxigenin-labeled RNA probes were synthesized, *in vitro*, using the SP6 polymerase riboprobe protocol (Amersham, Arlington Heights, MA). The Genius Nonradioactive Northern kit was from Boehringer Mannheim. Electrophoresis grade agarose was from FMC Corporation (Rockland, ME). Ampicillin, tetracycline, and chloramphenicol were from Sigma (St. Louis, MO).

E. coli vector. A *bop–atcase* chimeric gene was constructed for high-level expression (Fig. 2A). The expression vector was derived from pβgbop, which had previously been successful in directing high-level Bop expression in *E. coli* (18). pβgbop was linearized at the *bop* gene *Not*I site and blunt-ended by the addition of Klenow fragment and dNTPs. DNA encoding the *bop* gene 6 C-terminal amino acids (243–249), the translational stop codon, and 90 bases of noncoding sequence (including the *bop* gene major transcription terminator) was retained downstream of the *Not*I site. Following digestion at a unique internal *bop* gene *Sph*I site, the large vector fragment was gel purified. In a separate experiment, pβgbop was digested with *Sph*I and *Hae*II and the 217-bp internal *bop* gene fragment was gel purified. The coding region for the *E. coli* catalytic subunit of aspartyl transcarbamylase (*atcase*) was isolated from the cloning vector pEK17 (37) by simultaneous *Mse*I and *Nru*I digestion. An 845-bp fragment which contained all but the first 18 bp of the *atcase* gene coding region was isolated.

A linker for the two structural genes was constructed from two complementary synthetic oligonucleotides. The linker DNA sequence coded for 25 amino acids, including a proteinase Factor Xa site, and reconstructed the ATCase N-terminal coding region starting with amino acid 5 (38). Truncation of the first 4 amino

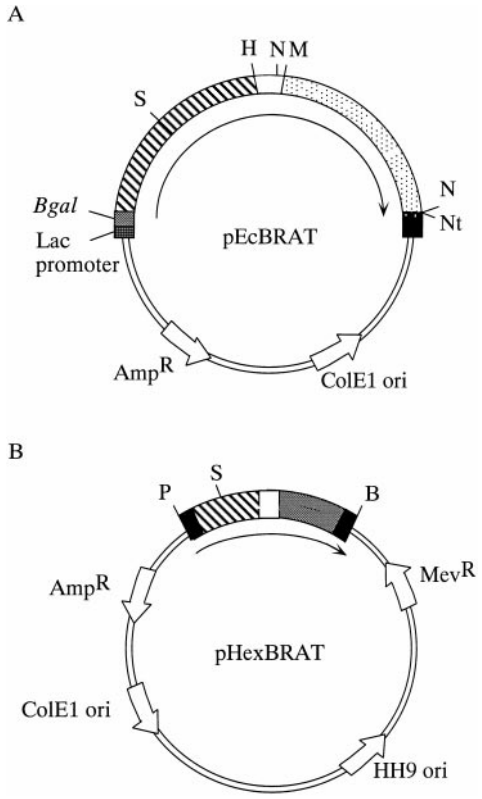

FIG. 2. BRAT expression vectors. The arrows indicate the direction of transcription and translation. The single letters designate DNA restrictions sites used in the cloning strategy: *Sph*I (S), *Hae*II (H), *Nru*I (N), *Mse*I (M), *Not*I (Nt), *Pst*I (P), and *Bam*HI (B). (A) *E. coli* expression vector pEcBRAT. Shown from 5′ to 3′ are the orientations of the Lac promoter, *Bgal*, *bop* gene, synthetic linker, and *atcase* gene coding sequences. (B) *H. salinarum* expression vector pHexBRAT. The orientation of the coding regions is the same as that for pEcBRAT. The filled upstream region contains the *H. salinarum bop* gene transcriptional promoter. The filled downstream region contains the *H. salinarum bop* gene translation terminator. pHexBRAT contains replicons (ori) derived from *E. coli* and *H. salinarum* and genes which confer resistance (R) to selectable markers ampicillin and mevinolin.

acids was rationalized since they were not involved in crystallographically determined ATCase secondary structure (39). The oligos were designed to contain 5′ *Hae*II and 3′ *Mse*I cloning sites and an internal diagnostic *Nru*I restriction site.

The synthetic oligos were annealed and all four DNA fragments were ligated simultaneously. The ligation mix was transformed into *E. coli* strain D1210 with ampicillin resistance as selectable marker. Clones were identified by nitrocellulose colony filter hybridization using a random-primed *atcase Mse*I–*Nru*I fragment as probe. A positive clone (named pEcBRAT) was confirmed by restriction mapping and DNA sequencing through cloning junctions.

H. salinarum vector (Fig. 2B). BRAT was expressed in *H. salinarum* under control of the wild-type *bop* gene promoter. A fragment containing the fused *bop* and *atcase* coding region sequences was isolated from pEcBRAT by PCR. The 5′ PCR oligo was complementary to sequences upstream of the internal *bop* gene *Sph*I site. The 3′ PCR oligo was complementary to sequences downstream of the *H. salinarum bop* gene major transcriptional terminator (maintained in the pEcBRAT construction) and included a *Bam*HI restriction site. The PCR fragment was digested with *Sph*I and *Bam*HI and gel purified. In a separate experiment the wild-type *bop* gene, previously cloned into pUC19 on a 1.2-kb *Pst*I–*Bam*HI fragment, was digested with *Sph*I and *Bam*HI to remove the 358-bp C-terminal half of the *bop* gene. The 1.2-kb fragment was previously isolated from *H. salinarum* strain R1 genomic DNA by PCR and contains transcriptional and translational regulatory sequences required for *bop* gene expression (15,40). The 358-bp *bop Sph*I–*Bam*HI fragment was replaced with the *bop–atcase Sph*I–*Bam*HI fragment. A positive clone was isolated and confirmed by restriction mapping and DNA sequencing and named pHsBRAT.

pHsBRAT was digested with *Pst*I and *Bam*HI and the *bop–atcase* chimeric gene was transferred into the *Pst*I/*Bam*HI cloning sites of the *E. coli*/*H. salinarum* shuttle vector pUBP2 (41) to generate the *H. salinarum* expression vector pHexBRAT.

Protein Expression and Purification

Buffers and reagents. ATCase purification buffer (APB) was 50 mM Tris base, 0.2 mM EDTA, 2 mM βME, and 250 mM NaCl, at pH 8.3. IPTG was from USB. Goat anti-rabbit IgG conjugated to alkaline phosphatase or peroxidase were from Sigma or Amersham. Alkaline phosphatase detection reagents (BCIP/NBT) were from Kirkegaard and Perry Labs (Gaithersburg, MD). ECL Western detection reagents were from Amersham. Detergents used included NG (Cal Biochem, San Diego, CA), SDS (Bio-Rad, Richmond, CA), Chapso and Chaps (Boehringer Mannheim Biochemicals), Tween 20 (Sigma), Triton X-100 (Pierce, Rockford, IL), and TDM (Anatrace, Maumee, OH). Four to twenty percent Tris–Glycine PAGE gels were purchased from NOVEX (San Diego, CA). Carbamyl phosphate and L-aspartate were from Sigma. 2,3-Butadionemonoxide and antipyrine for the ATCase colorimetric assay were from Eastman Kodak (Rochester, NY). Factor Xa (FXa) was from Boehringer Mannheim. Nitrocellulose membranes were from Schleicher and Schuell (Keene, NH). Immobilon-P transfer membranes were from Millipore (Bedford, MA). Hybond-ECL, Hybond-N, and Hybond-N^+ membranes were from Amersham.

Antibodies. BRAT expression was verified by immunodetection. The BR polyclonal antibodies used were described previously (18). Rabbit polyclonal antibodies against the catalytic subunit of ATCase were supplied by M. Wales (Texas A&M University). Antisera were absorbed to crude lysates of *E. coli* strain U39a and membranes isolated from *H. salinarum* strain L33. The antisera were clarified by centrifugation.

Quantification of BRAT. e-BOAT was quantified spectrophotometrically after regeneration of the BR domain by retinal addition (ϵ_{560} = 62,500 for purple membrane (42) and factoring in the BRAT calculated mass of 59.8 kDa). h-BRAT was quantified spectrophotometrically in membranes. ODs were recorded using a Shimadzu UV-160 spectrophotometer. Comparison between the dark adapted (DA) visible absorbance (at λ_{560}) and total protein UV absorbance (at λ_{280}) was used to assess BRAT purity (43).

e-BOAT expression and purification (Table 1). Fifty-liter pEcBRAT cultures were grown in a stainless steel Microgen SF-116 fermentor (New Brunswick Scientific Co.) and induced by addition of IPTG at an OD_{600} of 0.8. Cells were collected by centrifugation (25 min at 9500*g*, 4°C) 45 min postinduction. The yield was ~3.7 g, wet weight, of cells per liter of culture. Cell pellets were resuspended in 10 ml APB per liter of culture harvested. DNase I and RNase A were added to 2 μg/ml and the cells lysed by two passes through a French press at 6000 psi. Membranes were collected by centrifugation at 356,000*g* for 1 h. Crude membranes were fractionated into cytoplasmic and outer membrane components on sucrose step gradients (44) to determine the cellular location of e-BOAT accumulation. e-BOAT was purified as previously described for e-BO (43) with modifications. Diluted membranes were washed three times with APB and stripped in 40 mM Chaps overnight at 4°C. Stripped membranes were solubilized in 2% SDS (30 min with stirring) and clarified by centrifugation. e-BOAT was further purified by HPSEC using a 2.2 × 60-cm TSK G3000SW column. The mobile phase was 0.1% SDS, 100 mM sodium acetate, pH 6.0. Fractions containing e-BOAT were pooled and concentrated between column applications. Following the third successive size fractionation e-BOAT-containing samples were pooled for retinylation.

h-BRAT expression. pHexBRAT and pHexBR (containing the wild-type *bop* gene) (15,16) expression in *H. salinarum* was evaluated by a Western analysis of individual colonies. An aliquot of the transformation culture was diluted in peptone media and spread on solid selective media to yield 50–300 isolated colonies. The plates were grown at 42°C until individual colonies were visible. Colonies were absorbed to nitrocellulose filters and lysed in 1% SDS and washed for 15 min, with gentle agitation. Following 3 × 20-min washes (0.3% Tween 20) the filters were probed with BR or ATCase antibodies (1:10,000 dilution) overnight at 4°C. The filters were washed (3 × 20 min, 0.3% Tween 20) and probed with alkaline phosphatase-conjugated goat anti-rabbit secondary antibodies (1:20,000 dilution) for 5 h at 4°C. After three washes with Tris-buffered saline, pH 7.0, detection was accomplished with BCIP/NBT phosphatase substrates. Filters containing ET1001 and L33 colonies were used as positive and negative controls, respectively.

Further characterization of expression included DNA and RNA gel blot analyses. Individual colonies were used to inoculate 20 ml of selective peptone media and grown aerobically to OD_{660} ~ 1.2. Three 2-ml aliquots were harvested and cells pelleted by centrifugation. Cell pellets were frozen at −70°C prior to nucleic acid isolation.

Total *H. salinarum* DNA was isolated as described previously (16) and plasmid DNA was isolated by the Wizard Mini-Prep protocol. Southern analysis was performed on *Pst*I/*Bam*HI-digested DNA, blotted, and cross-linked to Hybond-N nylon membranes. Digoxigenin-11–dUTP was used for random-primed labeling of an *Alw*NI/*Not*I fragment containing the coding region for the nearly full-length *bop* gene or a *Pst*I/*Alw*NI fragment containing the upstream noncoding and the presequence coding regions. Membranes were exposed to X-OMAT film (Kodak) following incubation with alkaline phosphatase-conjugated anti-digoxigenin polyclonal antibody and dioxetane substrate (Lumi-Phos 530; Boehringer Mannheim).

Total *H. salinarum* RNA was extracted as described previously (16) and 2 μg was electrophoresed and transferred to Hybond-N^+ nylon membranes. A *Kpn*I/*Not*I fragment of the *bop* gene was cloned into the pSPT19-vector and digoxigenin-labeled dUTP RNA probes were transcribed *in vitro.* Detection followed the protocols of Engler-Blum (45). RNA blots were scanned and band intensities were quantified on an Alpha Innotech IS1000 digital imaging system.

Isolation of h-BRAT (Table 1). Individual *H. salinarum* colonies, containing pHexBRAT or pHexBR, were used to inoculate 20 ml of selective peptone medium and grown aerobically to an OD_{660} = 0.8. These cultures were used to inoculate 1 liter of peptone medium, prewarmed to 37°C in 3-liter Fernbach flasks and aerated by shaking at 250 rpm. Antifoam B (Baker, Phillipsburg, NJ) was added as required. At an OD_{660} = 1.2, cells were harvested and membranes were prepared according to Oesterhelt and Stoeckenius (46) except that cells were lysed by dialysis against 50 mM

NaCl and 20 mM Tris base, pH 8.0, at 4°C. Following one wash (100 mM NaCl and 20 mM Tris, pH 8.0) membranes were purified on linear sucrose gradients (25–45%, 50% cushion; 10 mM Tris, pH 8.0, 25°C). Membranes banding at the 50% cushion were collected and stored at 4 or −70°C. This material will be referred to as BRATM, for membranes containing purified BRAT, and as PM for membranes containing purified BR. Prior to use, sucrose was replaced by 10 mM Tris (pH 8) by centrifugation.

h-BOAT and h-BO monomers were prepared as described for e-BOAT except that 2 mM βME and boiling were included in the SDS solubilization procedure.

Retinylation of BOAT

Conditions for converting BOAT to BRAT upon addition of all-*trans*-retinal were adapted from standard protocols (43). BRAT was also retinylated in 60 mM acetate buffer containing 20 mM TDM and 0.06% SDS.

ATCase Activity

In vitro ATCase activity was evaluated by colorimetric (47) and radiographic methods (48). The assays were performed in 100 mM Tris, 0.2 mM EDTA, pH 7.4, 4.8 mM carbamyl phosphate, and 30 mM aspartate.

ATCase activity was tested *in vivo* by complementation. pEcBRAT and pβgbop were separately transformed into *E. coli* strain U39a ($\triangle$*pyrB*) and tested for growth on uracil-depleted media. Twenty-five-milliliter cultures of U39a, U39a-pEcBRAT, and U39a-pβgbop were grown to midlog phase ($OD_{600} \sim 0.4$) in YT medium. These were used to inoculate (1:1000) 25-ml cultures in SM-Glucose supplemented with 2 μM proline and 3 μM uracil. At an $OD_{600} = 0.8$ cells were harvested and washed twice in 10 ml of SM-Glucose and resuspended in 25 ml SM-Glucose. Aliquots (~200 cfu/plate) were spread on SM-Glucose complementation solid medium (Table 3) and incubated at 37°C. Each culture was separately spread on YT solid medium as a viability control.

Ultracentrifugation

The solubility, molecular mass, and number of protein molecules (BRAT or BR) per TDM mixed micelle was determined by equilibrium sedimentation. BRAT and BR samples were retinylated in TDM in 0, 50, 75, and 100% D_2O and diluted to $OD_{560} = 0.1–0.4$ in 20 mM TDM/D_2O. Samples were spun individually at 20K rpm, 4°C, in a Beckman Optima XLA analytical ultracentrifuge, equipped with absorbance optics. Solute transport was monitored by OD_{550} versus cell position and apparent molecular weight $[M_w(1 - \rho\nu)]$ was calculated according to $[(d\ln C/d\ln r^2)RT/\omega^2] = [M_w(1 - \rho_i\nu)_i]$, where M_w is the mixed micellar molecular weight, ν is the partial molar volume, C is the concentration of BRAT or BR (determined at OD_{560}), r is the cell pathlength, ρ_i is the solvent density at D_2O concentration i, and ω is the radial velocity of the rotor (49). The transport was considered to be at equilibrium when the calculated apparent molecular weight was within 1% on successive scans (Fig. 9). A global least squares analysis was performed on the equilibrium BRAT and BR data sets (last data points in Fig. 9) to determine M_w and ν.

Electron Microscopy

Membrane specimens for electron microscopy were prepared as described (50). PM and BRATM samples, at ~10 mM protein concentration in 10 mM Tris, pH 8.0, containing 40% (w/v) sucrose, were spread on electron microscope grids covered with collodion-supported carbon film. After the sample was allowed to settle for 90 s the grids were washed six times for 5 s each with 100 μl of distilled water to minimize sucrose. The specimens were embedded in uranyl formate and examined in a Philips CM12 electron microscope operated at 100 kV. Low-dose images (~10 el/Å^2) were recorded at 45,900 magnification and at 400–700 nm underfocus and were subsequently screened by optical diffraction. Image analysis and processing of the best preserved area from a single micrograph of BRATM were carried out using the MRC suite of programs, as described previously (50).

RESULTS

pEcBRAT Expression

e-BOAT expression was obtained upon IPTG induction of *E. coli* containing pEcBRAT (Fig. 3 and Table 1). e-BOAT was identified in cell lysates as a 60-kDa protein which reacted with antibodies raised separately against BR and ATCase (data not shown). Following induction of pβgbop, a single protein of 28 kDa, corresponding to e-BO, was found to react with the BR antibody only (18, this study). Membrane fractionation and subsequent SDS–PAGE analysis showed that e-BOAT was associated with the bacterial cytoplasmic membrane (data not shown).

Extensive screening of e-BOAT membranes with nondenaturing detergents failed to identify conditions which solubilized the fusion protein. As a result e-BOAT was subsequently solubilized and chromatographed in SDS (Fig. 4). e-BOAT eluted with a retention time significantly reduced from that for e-BO, consistent with its larger mass. Three consecutive HPSEC fractionations yielded e-BOAT at ~50% purity (Figs. 3A and 4).

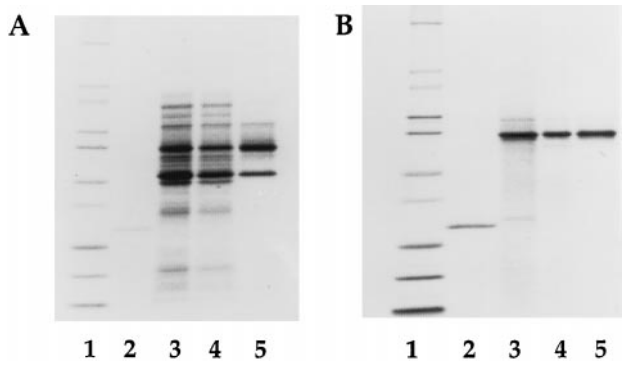

FIG. 3. SDS–PAGE of samples during the BRAT purification from (A) *E. coli* and (B) *H. salinarum*. Lane 1, molecular weight standards; lane 2, purified BR; lane 3, crude membranes; lane 4, Chaps-stripped membranes solubilized by 2% SDS in (A) and membranes purified by sucrose gradient centrifugation in (B); lane 5, BOAT following HPSEC in 0.1% SDS.

pHexBRAT Expression

pHexBRAT and pHexBR were expressed in *H. salinarum* to take advantage of the potential for obtaining a properly folded BR domain *in vivo* (Table 1). Transformants containing pHexBR were purple while pHexBRAT transformants were not. This was ultimately shown to result from lower levels of expression for BRAT. Southern analysis confirmed the presence of the pHex plasmids in all pHexBRAT and pHexBR cultures assayed and demonstrated that chromosomal recombination had not occurred (data not shown). An RNA gel blot analysis established that the *brat* gene was transcribed and that *brat* mRNA was reduced fourfold relative to *bop* mRNA at equivalent growth stages (Fig. 5). BRAT expression was subsequently confirmed by a Western analysis of individual pHexBRAT colonies using PM and ATCase antisera (data not shown). Following preparation of BRAT membranes purple color was observed, demonstrating that BR was properly folded as part of the fusion protein (Fig. 6). h-BR and h-BRAT formed membrane fractions which were isolated by sucrose density gradient centrifugation (PM and BRATM, respectively). PAGE analysis demonstrated that the PM and BRATM contained predominantly single proteins migrating at 25 and 60 kDa, respectively (Fig. 3B). Cross reactivity to the ATCase antisera in BRATM (and not to PM) established that the increase in size was a result of a fused ATCase domain (data not shown). Spectroscopic quantification of the PM and BRATM indicated yields of 20 and 7 mg, respectively, per liter of culture.

Extensive screening with nondenaturing detergents again failed to identify conditions which solubilized the BRATM. Following BRATM trypsinization, intact BR domains were quantitatively solubilized by treatment with Triton X-100 (data not shown). Subsequently, BRAT was solubilized in SDS and h-BOAT (formed due to the loss of retinal on SDS solubilization) was purified to homogeneity by one HPSEC fractionation (Figs. 3B and 4).

BRAT Characterization

BR activity. SDS-solubilized BOAT could be refolded with all-*trans*-retinal in 7 mM Chapso/DMPC or

TABLE 1

Purification and Characterization of the BRAT Protein

	E. coli	*H. salinarum*
Cell wet weight	3.7 g	2.5 g
Total membrane mass[a]	1.0 g	1.7 g
Cellular location	Inner membrane	Purple membrane
BR activity in membrane	No	Yes[b]
ATCase activity in membrane	Yes[c]	No[d]
Total mass of washed membrane[a]	870 mg[e]	250 mg[f]
Milligrams of BRAT and % purity in washed membrane	51 mg;[a] 15%[h]	7 mg;[b] >90%[h]
Milligrams of BRAT and % purity post HPSEC	13 mg;[g] 46%[h]	5 mg;[g] 100%[h]
Milligrams of BRAT and % purity following retinylation	5 mg;[b] 50%[h]	3 mg;[b] 100%[h]
Yield of BRAT[i]	9.8%	42%

[a] Pellet weight from 1 h of centrifugation at >100,000*g;* includes mass of lipids.
[b] Determined spectroscopically at 560 nm.
[c] Activity measured by an *in vivo* complementation assay.
[d] Colorimetric assay according to Pastra-Landis *et al.* (47).
[e] Refers to washed and Chaps-stripped membranes.
[f] Refers to isolated purple membrane.
[g] Determined by Bradford protein assay.
[h] Determined by densitometry of SDS–PAGE (see Fig. 3).
[i] Normalized to mass of BRAT in washed membranes.

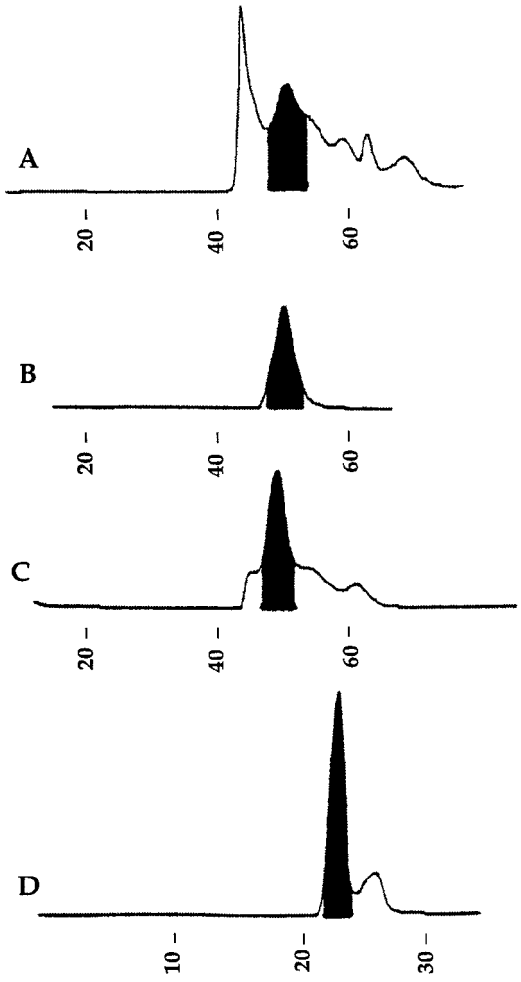

FIG. 4. HPSEC (TSK 0.75 × 60 cm for A, 22 × 60 cm for B, C, and D) elution profiles (280 nm optical density vs time (min) of Chaps-stripped *E. coli* membranes (A, B), purified BRATM (C), and PM (D). Membranes were solubilized in 2% SDS and chromatographed using a 0.1% SDS mobile phase. Fractions from (A) were pooled and chromatographed twice more to yield (B). Shaded areas in B, C, and D were used for retinylation, the results of which are in Table 2.

in 20 mM TDM (Table 2, Fig. 7). The half-time of refolding was similar to that of BR (Table 2). Following HPSEC removal of residual SDS and lipids, the A_{280}/A_{555} ratio for h-BRAT was 3.0, consistent with the additional ATCase mass in the fusion protein (relative to the BR ratio of 2.0; 44). The much higher A_{280}/A_{555} ratio for e-BRAT reflects the significant amounts of contaminating proteins remaining (Table 2, Figs. 3A and 4).

The spectroscopic properties of BR provided a convenient method to determine whether this domain was perturbed in BRAT. The ground state visible absorbance properties of BRAT are essentially the same as for BR. The mixed micelles containing BR and BRAT all possessed DA absorbance maxima near 555 nm

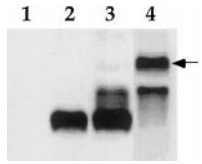

FIG. 5. RNA gel blot analysis of *H. salinarum* mRNA. *bop* and *brat* gene mRNAs were identified by hybridization with an *in vitro*-transcribed RNA probe consisting of a DNA fragment internal to the *bop* gene coding region. 2 μg of total RNA was analyzed from L33 (lane 1), L33 transformed with pHexBR (lane 2), ET1001 (lane 3), and L33 transformed with pHexBRAT (lane 4). *brat* mRNA is identified with an arrow. In a separate experiment *brat* mRNA was quantified by comparison to a serial dilution of *bop* mRNA isolated from L33 transformed with pHexBR (data not shown).

(Table 2, Figs. 6 and 7). In addition, both the dark-adapted PM and BRATM absorption maxima underwent a 10-nm red shift and a decrease in extinction coefficient upon light adaptation (Fig. 6).

ATCase activity. *In vivo* complementation confirmed that the ATCase domain of e-BOAT was capable of forming trimers (Table 3). The *E. coli* strain U39a (an obligate uracil auxotroph) transformed with pEcBRAT grew on uracil-depleted medium only if BOAT expression was induced, indicating trimerized and functional ATCase catalytic subunits. In contrast, following induction of the *E. coli* BO expression vector (pβgbop) U39a was unable to grow on uracil-depleted medium. Following either isolation of the BRATM or SDS solubilization and refolding of the BR domain of BRAT, ATCase activity was not observed. Purified *E. coli* catalytic subunits, assayed under identical conditions, displayed normal activity (data not shown). The engineered FXa proteinase site was inaccessible within

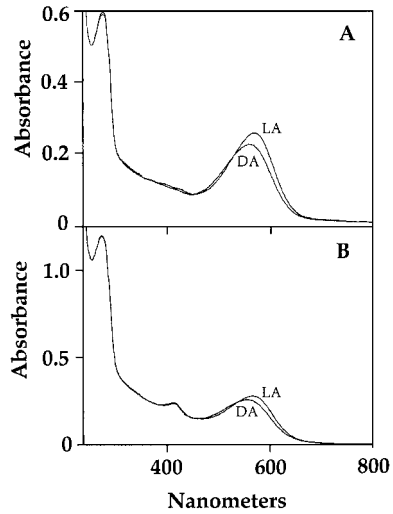

FIG. 6. Dark- (DA) and light-adapted (LA) absorption spectra of PM (A) and BRATM (B).

TABLE 2

Absorption Properties of BR and BRAT in 20 mM TDM

	λmax (nm)	$A_{280}/A_{\lambda max}$	$t_{1/2}$ retinylation (s)
EcBRAT	533	9.2	30
hBRAT	555	3.0	2.5
BR	555	2.0	1.5

the fusion construction, so that the BRAT catalytic domains could not be tested for activity independent of the BR domains.

Electron microscopy. Crystallographic analysis of images of the BRATM demonstrated that the fusion protein was trimeric in *H. salinarum*. The control PM samples consisted mostly of crystalline sheets which displayed the expected hexagonal, p3 symmetry (data not shown). A minor component of the BRATM contained crystalline sheets (maximum 0.5-μm diameter). The computed diffraction pattern of the BRATM sheets indicated a hexagonal lattice with dimensions of 65 Å. This is slightly larger than that observed for BR in native PM at −160°C (62.5 Å; 22, this study) and fused sheets (62.5 Å; 24) or BR in native PM at −120°C (61.9 Å; 23). The phases of significant spots in the computed transform of the BRATM crystal established a p3 symmetry for the lattice (average phase residual of 24°, to a resolution of 14 Å). This indicated that the trimeric association of BR was maintained in the BRATM. Figure 8 shows the computed reconstruction of BRAT in projection at a nominal resolution of 14 Å, overlaid with the outline of the BR envelope in PM. The phase origin (one of three for the p3 plane group) for the BRAT 2-D crystal was chosen such that the stain-excluding monomer density of BRAT best fit the projected monomer boundary for BR in PM (23). For this choice of phase origin, the symmetrized phases from the BRAT crystal differed by greater than 88° compared to the phases for PM (23,24). This may reflect structural perturbations resulting from the presence of the ATCase domain or an in-plane rotation of the fusion trimer with respect to PM. Since a goal of this work was to advance the three-dimensional X-ray analysis, BRATM crystalline sheets were not subjected to higher resolution analysis.

Solubility. Following HPSEC removal of residual SDS and DMPC from the Chaps/DMPC retinylation cocktail, BRAT was observed to precipitate over a period of weeks, at both room temperature and 4°C. The aggregated protein retained its purple color, indicating that the BR domain retained a near-native structure. BR remained soluble indefinitely under the same conditions (43, this study). At 4°C, in 20 mM TDM, BRAT remained soluble, with no change in visible absorbance

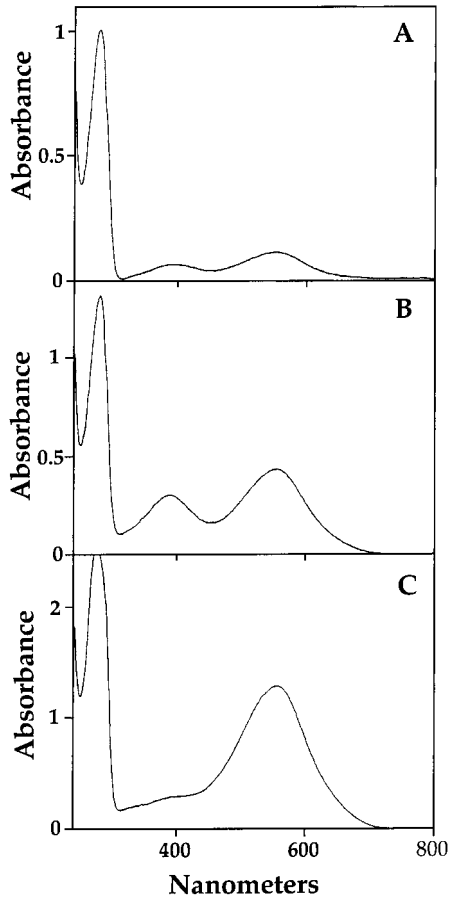

FIG. 7. Absorption spectra of retinylated BRAT from *E. coli* (A), *H. salinarum* (B), and BR (C), in 20 mM TDM.

properties, for greater than 30 days. Purple BRAT aggregates formed when the TDM concentration was brought below 20 mM. In contrast, BR remained soluble indefinitely in TDM concentrations as low as 5 mM.

TABLE 3

In Vivo Complementation Analysis of ATCase Activity

E. coli strain	Colony forming units					
	1	2	3	4	5	6
U39a	0	0	0	0	0	215 ± 47
U39a:BR	0	0	0	0	217 ± 63	181 ± 81
U39a:BRAT	0	0	0	220 ± 71	178 ± 26	236 ± 39

Note. Results are tabulated from three separate experiments. Numbers are reported as means and variances of the colony-forming units per plate. All media except No. 6 included ampicillin. The medium types were: (1) SM-Glucose, (2) SM-Glucose plus proline, (3) SM-Glucose plus uracil, (4) SM-Glucose plus proline and 1 mM IPTG, (5) SM-Glucose plus proline and uracil, and (6) complex *E. coli* medium (YT).

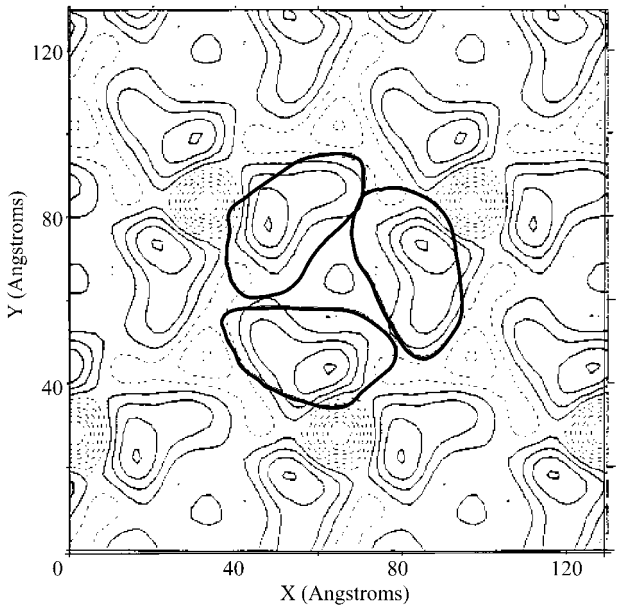

FIG. 8. A projected density map of BRATM crystals calculated at 14 Å resolution. The positive density (solid contours) represents protein while negative density represents lipid or stain-permeated regions. Each of the three approximately elliptical shapes (boldface) overlaying the three BRATM monomers represents the outer boundary of a BR monomer (23) positioned to generate maximum overlap with the BRATM monomers.

Equilibrium ultracentrifugation. A least-squares analysis of the equilibrium sedimentation profiles demonstrated that the BRAT–TDM and BR–TDM mixed micelles had molecular weights of 162 and 138 kDa, respectively (Fig. 9). The difference in molecular weights is consistent with the additional ATCase mass contained in BRAT. These data indicated that the mixed micelles contained a monomer of either BRAT or BR.

The limited set of detergents which maintained BRAT solubility was not found to be useful for crystallization. Crystallization trials in 20 mM TDM, with either BRAT or BR, resulted in detergent-phase transitions and the formation of precipitates possessing bleached BR domains.

DISCUSSION

Understanding the mechanism of action of transmembrane proteins relies on correlating function with structure. Syntheses of this type have been difficult due to the lack of success in determining high-resolution structures of membrane proteins. A major obstacle has been obtaining isotropic crystals useful for X-ray analysis. The handful of integral membrane proteins whose structures at atomic resolution have been solved suggests that protein–protein contacts may have contributed to the formation of well-ordered crystals. In the photoreaction center, the lattice contacts between neighboring complexes in the unit cell were formed by polar amino acid side chains involving the cytochrome subunit, the H-subunit, and to a minor extent the polar surface of the M subunit (1,2,51). In the light-harvesting complex, three protomer complexes were found per crystallographic asymmetric unit. All packing interactions were via protein–protein and protein–pigment contacts (4). Membrane association of the monotopic membrane protein prostaglandin H2 synthase occurs via lipid interaction with a hydrophobic patch composed of four amphipathic helices (8). The remainder of prostaglandin H2 synthase is extramembranous. The crystallographic asymmetric unit of prostaglandin H2 synthase was composed of two monomers which exhibited extensive protein contacts. In the crystals of porin trimers, two-dimensional layers formed through direct van der Waals interactions between hydrophobic side chains from the β-barrel walls. This resulted in type I membrane protein crystals in which the hydrophobic surface was not surrounded by a belt of detergent and direct contacts exist between proteins (6). These examples suggest that protein–protein interactions may be an important factor in crystal formation.

We have pursued a molecular engineering approach to increase the potential for protein-mediated lattice contacts in the crystallization of membrane proteins. We propose that chimeras of soluble proteins, or their

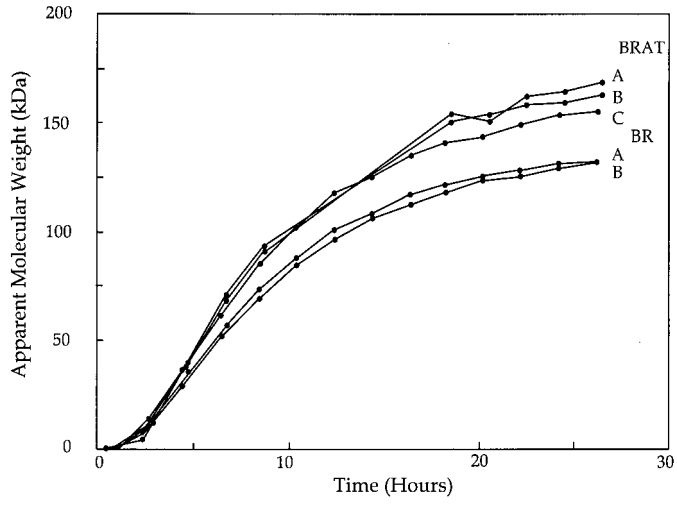

FIG. 9. Sedimentation analysis of BRAT and BR in 20 mM TDM. Mixed micelles were formed in solvents of differing densities, (A) 0 and (B) 50% D_2O for BR; (A) 0, (B) 50, and (C) 75% D_2O for BRAT. The samples were spun to near equilibrium in a Beckman XLA analytical ultracentrifuge. Protein concentration profiles, at various radii from the axis of rotation, were determined by absorbance at 550 nm (49) at the times indicated by the dots. Apparent molecular weights were calculated as described in the text and used to monitor the approach to equilibrium.

domains, and membrane proteins may provide lattice packing interactions which promote formation of well-ordered crystals. The fused polar domain would thus constitute a crystallization tag. This strategy is a more general case of that employed in antibody-based co-crystallization (52–54), which has been successfully applied to a membrane protein (9). Kaback and colleagues attempted a similar strategy by construction of fusions between the membrane protein lactose permease and the biotin acceptor domain of oxaloacetate decarboxylase or cytochrome b_{562} (55,56).

We chose to use BR as a test case since unlimited quantities can be obtained by transgenic expression. In addition, the extramembranous loops in BR are very short (24) and do not significantly contribute to crystal formation (27,28). To test whether additional extramembranous protein could aid three-dimensional crystal growth we fused a large polar domain to the BR C-terminus. The fusion partner was selected based on compatibility with BR tertiary and quaternary structure. We chose the catalytic subunit of aspartyl transcarbamylase as a potential crystallization tag since both BR and ATCase assemble into trimers, and the three-dimensional structures of the catalytic trimer (57) and holoenzyme have been determined (39,58). The trimers of BR and ATCase are roughly spherical with similar diameters (39,58). The molecular distances between the amino-termini of the ATCase monomers within an ATCase trimer (39) are nearly identical to those distances which relate the BR monomer carboxyl-termini within a BR trimer (24). The fusion of these two proteins therefore might not perturb their respective association properties. ATCase is an essential enzyme and homologues have been identified in Eubacteria, Eukaryotes, and Archaea (59,60). ATCase has been successfully overexpressed, in functional form, in *E. coli* (37). Thus, expression was not anticipated to adversely affect *H. salinarum* viability, allowing production of fusion protein in the quantities required for purification and crystallization.

Molecular Strategy

Our previous experience with *bop* gene expression guided the fusion strategy. Successful expression in *E. coli* was dependent on a 12-amino-acid βgal N-terminal fusion, present in pβgbop (18). In *H. salinarum* the *bop* gene N-terminal coding region contains a Shine–Dalgarno ribosome binding sequence (13) and a presequence signal which directs cotranslational membrane insertion (61). BR function was not perturbed by papain truncation of the C-terminus (62) and diffraction analysis indicated that the BR C-terminus is not ordered (63). We thus reasoned that a C-terminal fusion might not disrupt determinants of high-level expression or the structure of BR. Additionally, the C-terminus of BR is cytoplasmic in *H. salinarum;* since ATCase is a cytoplasmic enzyme C-terminal fusion was chosen to maximize the potential of producing functional protein.

We successfully constructed and expressed BRAT, at high levels, in both *E. coli* and *H. salinarum*. There were three distinct advantages to expressing the fusion protein in *H. salinarum*. First, the BR domain was properly folded and inserted into the membrane. Second, BRAT formed a membrane fraction, *in vivo,* which was isolated by sucrose density centrifugation. Subsequent purification and spectroscopic analysis was expedited by the isolation of this membrane fraction. Finally, the BRATM contained two-dimensional crystals, allowing structural characterization by electron microscopy.

Domain Properties

The BO domain of BRAT refolded quantitatively upon addition of retinal. The time course of the reaction was similar to that of wild-type BR, indicating that the folding proceeded independent of the hydrophilic ATCase domain. This observation is consistent with the two-state models proposed to describe the folding of membrane proteins, in which hydrophobic (e.g., protein–lipid bilayer) and polar (protein–protein) interactions form independently (64). In addition, the ground-state visible absorbance properties of BRAT were comparable to those of BR. Therefore, the BR domain was minimally perturbed by fusion with ATCase and would be expected to resemble the ground-state structure of wild-type BR (24).

As demonstrated by electron microscopy and image processing the ATCase domain formed trimers, suggesting that the monomers possessed sufficient tertiary structure to allow native subunit association properties. The orientation of chimeric trimers was altered compared to BR in the PM, which may be a consequence of the fusion or a property of the ATCase domain. The *in vivo* complementation study demonstrated that ATCase activity resulted from e-BOAT expression. Thus catalytic trimers had formed (29,30) in the presence of an unfolded BO domain. However, no ATCase activity was observed upon isolation of membranes, or following refolding of the BR domain, *in vitro*. The ATCase active site is composed of amino acid side chains originating from both sides of a monomer–monomer interface (39,58). Steric perturbations, resulting from close apposition with BR, may have propagated along this interface, leading to the loss of activity. Such a tight association is supported by the observation that the FXa site engineered into the

linker region between the two domains was inaccessible to the proteinase.

In sum, ATCase and BR can assume near-native tertiary and quaternary structures as components of the fusion protein. The fusion proteins generated by Kabach and colleagues also retained biochemical features intrinsic to the individual domains (55,56). The apparent independence of polar and nonpolar domains, in these examples, is consistent with the dissimilar energetic forces predicted to stabilize water-soluble and transbilayer proteins (65).

BRAT Solubilization and Crystallization Trials

Since both BR and ATCase were able to assume near-native conformations we pursued BRAT solubilization and purification with aim of crystallization. However, the ATCase domain inhibited solubilization of BRAT in nondenaturing detergents. Following solubilization in SDS and regeneration of BR with retinal, the Chaps/DMPC/SDS or TDM cocktails were the only conditions which maintained BRAT solubility and BR stability. Ultracentrifugation demonstrated that BRAT existed as monomers in TDM micelles, accounting for the lack of ATCase enzymatic activity. The TDM–BRAT micelles also possessed a large total mass with high TDM-to-protein ratios. Lowering TDM, or SDS, concentrations resulted in the irreversible formation of purple precipitates. The insolubility of BRAT micelles is most likely due to exposed ATCase interfaces. The interfaces between monomers, within an ATCase trimer, are composed of predominantly nonpolar amino acids (39). Alwell and colleagues estimated the Gibbs free energy of dissociating the ATCase trimer to be 7–10 kcal per interface (66). Exposure of these interfaces is energetically unfavorable and they would readily associate with available nonpolar surfaces. The large micelle size and high detergent concentrations may have been required to solvate the nonpolar ATCase interfaces and inhibit aggregation (39,58). The high detergent concentrations have hindered the crystallization of BRAT. Further crystallization trials will require identification of detergent/lipid combinations which do not result in uncontrolled fusion protein aggregation.

Crystallization Tag Strategy

The use of soluble proteins, or domains, as crystallization tags extends current fusion strategies which have proven useful for protein detection and purification (67,68). Here we report the expression and purification of a BR chimera designed to test this new crystallization strategy. We desired to engineer a membrane protein with a higher proportion of polar surface area, potentially stabilizing the BR trimer, enhancing solubilization, and mediating the formation of crystal packing contacts. Our efforts with BRAT identify criteria to be considered for selection of future tag candidates. These criteria include the effects of detergents on fusion protein solubility and stability. Additional insights regarding a similar approach have been put forward by Kabach and colleagues (56).

All fusions containing membrane protein domains require solubilization and purification in the presence of detergents. The effectiveness of a tag domain will depend on the influence of detergent additives on its activity and stability. The effect of detergent on ATCase oligomerization in BRAT illustrates this point. Our original strategy was to stabilize, solubilize, and crystallize BR trimers. However, solubilization and reconstitution yielded BRAT monomers, which have not been useful for three-dimensional crystallography. The effect of detergents on the structure and function of soluble proteins, or their domains, has not been systematically tested. Approximately 40 soluble proteins have been crystallized in the presence of detergent additives (69). The detergent β-octyl glucoside has been the most frequently used, in concentrations well below its critical micelle concentration (70). These detergent concentrations do not replicate those used in solubilization, purification, and crystallization trials of membrane proteins. The best indication that soluble domains may retain useful properties in the presence of detergents comes from the determination of membrane protein three-dimensional structures. The photoreaction centers, light-harvesting complexes, prostaglandin H2 synthase, and cytochrome *c* oxidase all have large hydrophilic domains which were highly ordered in detergents (1,2,8,9). Thus, engineered polar domains may also retain native properties under the detergent conditions required for purification and crystallization.

Obtaining X-ray-quality crystals requires large quantities of protein. The handful of transmembrane proteins whose structures at atomic level have been determined relied on proteins obtained from highly abundant natural sources. In contrast, the majority of membrane proteins are found naturally in such limited quantities that their purification and crystallization are not possible. By definition, the chimeric approach is nonnative. Pursuing the tag approach therefore requires expression systems appropriate for both the tag and the membrane protein domains.

Useful heterologous overexpression systems would greatly enhance the potentials of the crystallization tag strategy. Such systems are generally not available for membrane proteins (for reviews see 71, 72). The work presented is the first example of the high-level expression of nonnative proteins in the Archaea. Since the codon usage biases for *E. coli* ATCase and BR are 50

and 70% GC, respectively, high-level expression might not have been predicted. Our work demonstrates that the regulon controlling *bop* gene expression in *H. salinarum* (15,16,34) may be uniquely appropriate for expressing BR fusion proteins, and possibly membrane proteins in general, in the quantities required for structural analysis.

ACKNOWLEDGMENTS

The authors gratefully acknowledge J. Wild and M. Wells for supplying ATCase polyclonal antibodies, H. K. Schachman for supplying purified ATCase catalytic subunits and giving generous assistance with ATCase activity assays, and N. E. Kantrowitz for providing plasmid pEK17. In addition, we thank N. Alwell and S. Bromberg for helpful ATCase discussions and, finally, Dr. R. Shand and Dr. B. Moss for critically reading the manuscript.

REFERENCES

1. Allen, J. P., Feher, G., Yeates, T. O., Komiya, H., and Rees, D. C. (1987) Structure of the reaction center from *Rhodobacter sphaeroides* R-26: The cofactors. *Proc. Natl. Acad. Sci. USA* **84,** 5730–5734.
2. Deisenhofer, J., and Michel, H. (1989) The photosynthetic reaction centre from the purple bacterium *Rhodobacter sphaeroides*. *EMBO J.* **8,** 2149–2170.
3. Chang, C.-H., El-Kabbani, O., Tiede, D., Norris, J., and Schiffer, M. (1991) Structure of the membrane-bound protein photosynthetic reaction center from *Rhodobacter sphaeroides*. *Biochemistry* **30,** 5352–5360.
4. McDermott, G., Prince, S. M., Freer, A. A., Hawthornthwaite, A. M., Papiz, M. Z., Cogdell, R. J., and Isaacs, N. W. (1995) Crystal structure of an integral membrane light-harvesting complex from photosynthetic bacteria. *Nature* **374,** 517–521.
5. Weiss, M. S., Dreusch, A., Schiltz, U., Nestel, U., Welte, W., Weckesser, J., and Schulz, G. E. (1991) The structure of porin from *Rhodobacter capsulatus* at 1.8A resolution. *FEBS Lett.* **280,** 379–382.
6. Cowan, S. W., Schirmer, T., Rummel, G., Steiert, X., Ghosh, R., Pauptit, R. A., Jansonius, J. N., and Rosenbusch, J. P. (1992) Crystal structures explain functional properties of two *E. coli* porins. *Nature* **358,** 727–733.
7. Kreusch, A., Neubuser, A., Schiltz, E., Weckesser, J., and Schulz, G. E. (1994) Structure of the membrane channel porin form *Rhodopseudomonas blastica* at 2.0Å resolution. *Protein Sci.* **3,** 58–63.
8. Picot, D., Loll, P. J., and Garavito, R. M. (1994) The 3.1Å X-ray structure of an integral membrane enzyme prostaglandin H2 synthase-1. *Nature* **367,** 243–249.
9. Ostermeier, C., Iwata, S., Ludwig, B., and Michel, H. (1995) Fv fragment-mediated crystallization of the membrane protein bacterial cytochrome c oxidase. *Nat. Struct. Biol.* **2,** 842–846.
10. Doyle, D. A., Cabral, J. M., Pfuetzner, R. A., Kuo, A., Gulbis, J. M., Cohen, S. L., Chait, B. T., and MacKinnon, R. (1998) The structure of the potassium channel: Molecular basis of K^+ conduction and selectivity. *Science* **280,** 69–77.
11. Oesterhelt, D., and Stoekenius, W. (1973) Functions of a new photoreceptor membrane. *Proc. Natl. Acad. Sci. USA* **70,** 2853–2857.
12. Oesterhelt., D., and Krippahl, G. (1983) Phototrophic growth of halobacteria and its use for isolation of photosynthetically-deficient mutants. *Ann. Microbiol. (Inst. Pasteur)* **134B,** 137–150.
13. Dunn, R., McCoy, J., Simsek, M., Majumdar, A., Chang, S., RajBhandary, U., and Khorana, H. G. (1981) The bacteriorhodopsin gene. *Proc. Natl. Acad. Sci. USA* **78,** 6744–6748.
14. Ni, B. F., Chang, M., Duschl, A., Lanyi, J., and Needleman, R. (1990) An efficient system for the synthesis of bacteriorhodopsin in *Halobacterium halobium*. *Gene* **90,** 169–172.
15. Turner, G. J., Miercke, L. J. W., Thorgeirsson, T. E., Kliger, D. S., Betlach, M. C., and Stroud, R. M. (1993) Bacteriorhodopsin D85N: Three spectroscopic species in equilibrium. *Biochemistry* **32,** 1332–1337.
16. Winter-Vann, A. M., Martinez, L. C., Parker, L., Talbot, J. D., and Turner, G. J. (1999) Transgenic membrane protein expression in a HaloArcheon: The stability of protein expression. *Cancer Res. Ther. and Control* **8,** 275–289.
17. Karnik, S., Nassal, M., Doi, T., Jay, E., Sgaramella, V., M., and Khorana, H. G. (1987) Structure–function studies on bacteriorhodopsin. II. Improved expression of the bacterio-opsin gene in *E. coli*. *J. Biol. Chem.* **262,** 9255–9263.
18. Shand, R. F., Miercke, L. J. W., Mitra, A. K., Fong, S. K., Stroud, R. M., and Betlach, M. C. (1991) Wild-type and mutant bacterioopsins D85N, D96N, and R82Q: High-level expression in *Escherichia coli*. *Biochemistry* **30,** 3082–3088.
19. Mathies, R. A., Lin, S. W., Ames, J. B., and Pollard, W. T. (1991) From femtoseconds to biology: Mechanism of bacteriorhodopsin's light-driven proton pump. *Annu. Rev. Biophys. Biophys. Chem.* **20,** 491–518.
20. Ebrey, T. (1993) Light energy transduction in bacteriorhodopsin, *in* "Thermodynamics of Membrane Receptors and Channels" (Jackson, M. B., Ed.), pp. 353–387, CRC Press, Boca Raton, FL.
21. Lanyi, J. K. (1992) Proton transfer and energy coupling in the bacteriorhodopsin photocycle. *J. Bioenerg. Biomembr.* **24,** 169–179.
22. Henderson, R., and Unwin, P. N. (1975) Three-dimensional model of purple membrane obtained by electron microscopy. *Nature* **257,** 28–32.
23. Hayward, S. B., and Stroud, R. M. (1981) Projected structure of purple membrane determined to 3.7Å resolution by low temperature electron microscopy. *J. Mol. Biol.* **151,** 491–517.
24. Grigorieff, M., Ceska, T. A., Downing, K. H., Baldwin, and Henderson, R. (1996) Electron crystallographic refinement of the structure of bacteriorhodopsin. *J. Mol. Biol.* **259,** 393–421.
25. Michel, H., and Oesterhelt, D. (1980) Three-dimensional crystals of membrane proteins: Bacteriorhodopsin. *Proc. Natl. Acad. Sci. USA* **77,** 283–1285.
26. Schertler, G. F. X., Bartunik, H. D., Michel, H., and Oesterhelt, D. (1993) Orthorhombic crystal form of bacteriorhodopsin nucleated on benzamidine diffracting to 3.6 A resolution. *J. Mol. Biol.* **234,** 156–164.
27. Landau, E. M., and Rosenbusch, J. P. (1996) Lipid cubic phases: A novel concept for the crystallization of membrane proteins. *Proc. Natl. Acad. Sci. USA* **93,** 14532–14535.
28. Luecke, H., Richter, H.-T., and Lanyi, J. K. (1998) Proton transfer pathways in bacteriorhodopsin at 2.3 angstrom resolution. *Science* **280,** 1934–1937.
29. Burns, D. L., and Schachman, H. K. (1982) Assembly of the catalytic trimers of aspartate transcarbamoylase from folded monomers. *J. Biol. Chem.* **257,** 8638–8647.
30. Burns, D. L., and Schachman, H. K. (1982) Assembly of the catalytic trimers of aspartate transcarbamoylase from unfolded polypeptide chains. *J. Biol. Chem.* **257,** 8648–8654.

31. Kuhn, I., Stephenson, F. H., Boyer, H. W., and Greene, P. J. (1986) Positive-selection vectors utilizing lethality of *Eco*RI endonuclease. *Gene* **42,** 253–263.
32. Stoeckenius, W., and Kanau, W. H. (1968) Further characterization of particulate fractions from lysed cell envelopes of *Halobacterium halobium* and isolation of gas vacuole membranes. *J. Cell Biol.* **38,** 337–357.
33. Wagner, G., Oesterhelt, D., Krippahl, G., and Lanyi, J. (1983) Bioenergetic role of halorhodopsin in *Halobacterium halobium* cells. *FEBS Lett.* **131,** 341–345.
34. Betlach, M. C., and Shand, R. F. (1991) Molecular biology and regulation of bacterio-opsin gene expression in *Halobacterium halobium*, *in* "General and Applied Aspects of Halophilic Microorganisms" (Rodriguez-Valera, F., Ed.), pp. 259–264, Plenum, New York.
35. Miller, J. H. (1972) "Experiments in Molecular Genetics," pp. 433, Cold Spring Harbor Laboratory Press, Cold Spring Harbor, NY.
36. Davis, R. W., Botstein, D., and Roth, J. R. (1980) "Advanced Bacterial Genetics," pp. 203–204, Cold Spring Harbor Laboratory Press, Cold Spring Harbor, NY.
37. Nowlan, S. F., and Kantrowitz, E. R. (1985) Superproduction and rapid purification of *Escherichia coli* aspartate transcarbamylase and its catalytic subunit under extreme derepression of the pyrimidine pathway. *J. Biol. Chem.* **260,** 14712–14716.
38. Hoover, T. A., Roof, W. D., Foltermann, K. F., O'Donovan, G. A., Bencini, D. A., and Wild, J. (1983) Nucleotide sequence of the structural gene (pyrB) that encodes the catalytic polypeptide of aspartate transcarbamoylase of *Escherichia coli. Proc. Natl. Acad. Sci. USA* **80,** 2462–2466.
39. Ke, H., Lipscomb, W. N., Cho, Y., and Honzatko, R. B. (1988) Complex of *N*-phosphoacetyl-L-aspartate carbamoyltransferase. X-ray refinement, analysis of conformational changes and catalytic and allosteric mechanisms. *J. Mol. Biol.* **240,** 725–747.
40. Gropp, F., Gropp, R., and Betlach, M. C. (1995) Effects of upstream deletions on light- and oxygen regulated bacterio-opsin gene expression in *Halobacterium halobium*. *Mol. Microbiol.* **16,** 357–364.
41. Blaseio, U., and Pfeifer, F. (1990) Transformation of *Halobacterium halobium:* Development of vectors and investigation of gas vesicle synthesis. *Proc. Natl. Acad. Sci. USA* **86,** 5478–5482.
42. Rehorek, M., and Heyn, M. P. (1979) Binding of all-*trans*-retinal to the purple membrane. Evidence for cooperativity and determination of the extinction coefficient. *FEBS Lett.* **18,** 4977–4983.
43. Miercke, L. J., Betlach, M. C., Mitra, A. K., Shand, R. F., Fong, S. K., and Stroud, R. M. (1991) Wild-type and mutant bacteriorhodopsins D85N, D96N, and R82Q: purification to homogeneity, pH dependence of pumping, and electron diffraction. *Biochemistry* **30,** 3088–3089.
44. Osborn, M. J., Gander, J. E., Parisi, E., and Carson, J. (1972) Mechanism of assembly of the outer membrane of *Salmonella typhimurium*. Isolation and characterization of cytoplasmic and outer membrane. *J. Biol. Chem.* **247,** 3962–3972.
45. Engler-Blum, G., Meie, M., Frank, J., and Muller, G. A. (1993) Reduction of background problems in nonradioactive Northern and Southern blot analyses enables higher sensitivity than ^{32}P-based hybridizations. *Anal. Biochem.* **210,** 235–244.
46. Oesterhelt, D., and Stoeckenius, W. (1974) Isolation of the cell membrane of *Halobacterium halobium* and its fractionation into red and purple membrane. *Methods Enzymol.* **31,** 667–678.
47. Pastra-Landis, S. C., Foote, J., and Kantrowitz, E. R. (1981) An improved colorimetric assay for aspartate and ornithine transcarbamylases. *Anal. Biochem.* **118,** 358–363.
48. Davies, G. E., Vanaman, T. C., and Stark, G. R. (1970) Aspartate transcarbamylase. *J. Biol. Chem.* **245,** 1175–1179.
49. Cantor, C. R., and Schimmel, P. R. (1980) "Biophysical Chemistry," Part II, Freeman, New York.
50. Mitra, A. K., Miercke, L. J., Turner, G. J., Shand, R. F., Betlach, M. C., and Stroud, R. M. (1993) Two-dimensional crystallization of *Escherichia coli*-expressed bacteriorhodopsin and its D96N variant: High resolution structural studies in projection. *Biophys. J.* **65,** 1295–1306.
51. Chang, C.-H., Tiede, D., Tan, J., Smith, U., Norris, J., and Schiffer, M. (1986) Structure of *Rhodopseudomonas sphaeroides* R-26 reaction center. *FEBS Lett.* **205,** 82–86.
52. Arevalo, J. H., Hassig, C. A., Stura, E. A., Sims, M. J., Taussig, M. J., and Wilson, I. A. (1994) Structural analysis of antibody specificity. Detailed comparison of five Fab′-steroid complexes. *J. Mol. Biol.* **241,** 663–690.
53. Clark, A. D., Jcobo-Molina, A., Clark, P., Hughes, S. H., and Arnold, E. (1995) Crystallization of human immunodeficiency virus type 1 reverse transcriptase with and without nucleic acid substrates, inhibitors, and an antibody Fab fragment. *Methods Enzymol.* **262,** 171–185.
54. Li, H., and Lawson, C. L. (1995) Crystallization and preliminary X-ray analysis of *Borrelia burgdorferi* outer surface protein A (OspA) complexed with a murine monoclonal antibody Fab fragment. *J. Struct. Biol.* **115,** 335–337.
55. Consler, T. G., Persson, B. L., Jung, H., Zen, K. H., Jung, K., Prive, G. G., Verner, G. E., and Kaback, H. R. (1993) Properties and purification of an active biotinylated lactose permease from *Escherichia coli. Proc. Natl. Acad. Sci. USA* **90,** 6934–6938.
56. Prive, G. G., Verner, G. E., Weitzman, C., Zen, K. H., Eisenberg, D., and Kaback, H. R. 1994. Fusion proteins as tools for crystallization: The lactose permease from *Escherichia coli. Acta Crystallogr.* **50,** 375–379.
57. Stevens, R. C., Reinisch, K. M., and Lipscomb, W. N. (1991) Molecular structure of *Bacillus subtillis* aspartate transcarbamoylase at 3.0Å resolution. *Proc. Natl. Acad. Sci. USA* **88,** 6087–6091.
58. Kim, K. H., Pan, Z., Honzatko, R. B., Ke, H., and Lipscomb, W. N. (1987) Structural asymmetry in the CTP-liganded form of aspartate carbamoyltransferase. *J. Mol. Biol.* **196,** 853–875.
59. Wild, J. R., and Wales, M. E. (1990) Molecular evolution and genetic engineering of protein domains involving aspartate transcarbamoylase. *Annu. Rev. Microbiol.* **44,** 193–218.
60. Bult, C. J., White, O., Olsen, G. J., Zhou, L., Fleischmann, R. D., Sutton, G. G., Blake, J. A., FitzGerald, L. M., Clayton, R. A., Gocayne, J. D., Kerlavage, A. R., Dougherty, B. A., Tomb, J. F., Adams, M. D., Reich, C. I., Overbeek, R., Kirkness, E. F., Weinstock, K. G., Merrick, J. M., Glodek, A., Scott, J. L., Geoghagen, N. S. M., and Venter, J. C. (1996) Complete genome sequence of the methanogenic Archaeon, *Methanococcus jannaschii. Science* **273,** 1058–1073.
61. Gropp, R., Gropp, F., and Betlach, M. C. (1995) Association of the halobacterial 7s RNA to the polysome correlates with expression of the membrane protein bacteriorhodopsin. *Proc. Natl. Acad. Sci. USA* **89:** 1204–1208.
62. Ovchinnikov, Y. A., Abdulaev, N. G., Kiselev, A. V., Drachev, L. A., Kaulen, A. D., and Skulachev, V. P. (1986) The water-exposed C-terminal sequence of bacteriorhodopsin does not affect H^+ pumping. *FEBS Lett.* **194,** 16–20.

63. Wallace, B. A., and Henderson, R. (1982) Location of the carboxyl terminus of bacteriorhodopsin in purple membrane. *Biophys. J.* **39,** 233–239.

64. Popot, J.-L., and Engleman, D. M. (1990) Membrane protein folding and oligomerization: The two-stage model. *Biochemistry* **29,** 4029–4037.

65. Haltia, T., and Freire, E. (1995) Forces and factors that contribute to the structural stability of membrane proteins. *Biochim. Biophys. Acta* **1228,** 1–27.

66. Bromberg, S., Licata, A., Mallikarachchi, D., and Allewell, N. M. (1994) Ligation alters the pathway of urea-induced denaturation of the catalytic trimer of *Escherichia coli* aspartate transcarbamylase. *Protein Sci.* **3,** 1236–1244.

67. Kolodziej, P. A., and Young, R. A. (1991) Epitope tagging and protein surveillance. *Methods Enzymol.* **194,** 508–519.

68. Ford, C. L., Suominen, I., and Glatz, C. E. (1991) Fusion tails for recovery and purification of recombinant proteins. *Protein Expression Purif.* **2,** 95–107.

69. Gilliland, G. L, Tung, M., Blakeslee, D. M., and Ladner, J. (1994) The biological macromolecule crystallization database, Version 3.0: New features, data, and the NASA archive for protein crystal growth data. *Acta Crystallogr.* **D50,** 408–413.

70. McPherson, A., Koszelak, S., Axelrod, H., Day, J., Williams, R., Robinson, L., McGrath, M., and Cascio, D. (1986) An experiment regarding crystallization of soluble proteins in the presence of beta-octyl glucoside. *J. Biol. Chem.* **261,** 1969–1975.

71. Schertler, G. F. X. (1992) Overproduction of membrane proteins. *Curr. Opin. Struct. Biol.* **2,** 534–544.

72. Grisshammer, R., and Tate, C. G. (1995) Overexpression of integral membrane proteins for structural studies. *Q. Rev. Biophys.* **28,** 315–422.